Hindawi Publishing Corporation
Advances in Materials Science and Engineering
Volume 2011, Article ID 767260, 6 pages
doi:10.1155/2011/767260

Research Article

Influence of Welding Parameters on Weld Formation and Microstructure of Dual-Laser Beams Welded T-Joint of Aluminum Alloy

Min Li,[1] Zhuguo Li,[1] Yong Zhao,[1] Hao Li,[2] Yuhua Wang,[2] and Jian Huang[1]

[1] *Shanghai Key Laboratory of Materials Laser Processing and Modification, Shanghai Jiao Tong University, Shanghai 200240, China*
[2] *Shanghai Aircraft Manufacturing Co., Ltd. Shanghai 200436, China*

Correspondence should be addressed to Jian Huang, jhuang@sjtu.edu.cn

Received 15 March 2011; Revised 24 May 2011; Accepted 26 May 2011

Academic Editor: J. Dutta Majumdar

This paper focused on the welding 1.8 mm thick 6061 aluminum alloy plates in T-joint form using dual lasers that introduced by a Nd: YAG laser and a CO_2 laser with 4043 aluminum filler wire. The effects of welding parameters on the T-joint weld appearance, microstructure and the joint mechanical properties were studied systematically, The influence of welding parameters included the distance between two laser beams, welding speed, laser power and the laser beam offset toward the stringer. The weld appearance, microstructure, hardness of the joint were evaluated by optical microscope and micro-hardness test. A monotonic quasi-static tensile test was conducted by a self-made clamping device to obtain the tensile property of welded joints. At the optimized parameters, the welded T-joint showed good weld appearance without macro defects; the micro hardness of welds ranged from 75 to 85 $HV_{0.3}$, and the tensile strength was about 254 MPa with the fracture at the heat affected zone on the stringer side.

1. Introduction

From the viewpoint of demand for weight loss in aerospace industry, joint, of fuselage panels connected by traditional mechanical fastening will be replaced by laser beam welding [1]. Laser beam welding provides outstanding characteristics of high energy density, high welding speed, high flexibility of the moving system, low distortions, narrow heat affected zone, and high depth-to-width ratio [2–4]. However, T-joint of fuselage panels welded at one side by full penetration will cause distortions because of the asymmetric force. Distortions not only increase the difficulty of frock clamping, but also add the probability of crack [5–7]. In past decades, mitigation methods have been developed to reduce welding distortion using different approaches, such as low-stress no-distortion welding with additional cooling [8], predeformation [9], thermal tensioning [10], optimized welding sequences [11], or change clamping support distance [12]. Those methods are capable of reducing the distortion of T-joint, however, dual-beam laser welding synchronously at two sides can minimize the formation of weld-induced self-stresses in the weld seams because of the symmetrical stress distribution. In essential, dual beam laser weld T-joint is a more efficient way to weld T-joint configuration. Up to now, the influence of welding parameters on weld formation and microstructure of T-joint welded by dual laser beams was seldom reported, especially for thin aluminum alloy plates. So this paper focuses on the welding of 1.8 mm thin aluminum alloy plate T-joints synchronously at two sides. The main goal is to evaluate the effects of welding parameters on the microstructures and joint mechanical properties systematically. Welding parameters include the distance between two laser beams, welding speed, laser power, and the laser beam offset toward the stringer (BOF).

2. Materials and Method

Test plates used in this study were the age-hardened (T6) 6061 aluminum alloy with the thickness of 1.8 mm. The weld seam between the stringers and the fuselage skin were simultaneously welded from both sides of the stringer by means of a dual-beam system. The dual-beam system is composed

Table 1: Nominal chemical composition of materials used (wt.%).

	Si	Fe	Cu	Mn	Mg	Cr	Zn	Ti	Al
6061	0.4–0.8	0.7	0.15–0.4	0.15	0.8–1.2	0.10	0.25	0.15	Balance
4043	4.5–6.0	<0.8	0.30	0.05	0.05	—	0.10	<0.02	Balance

of a 15 kW continuous wave (cw) CO_2 laser TLF15000 of TRUMPF and a 3 kW cw Nd:YAG laser LS-YC of IHI with spot sizes of 0.86 mm and 0.9 mm, respectively. YAG laser beam is in multimode, CO_2 laser beam is of low-order mode. The dual beam lasers were fixed together with the self-designed fixture system to ensure synchronism. During the laser processing, pure helium gas was used as the shielding gas, which was coaxial ejected with the laser beams. The flow rates are 15 and 28 L/min at the sides of Nd:YAG laser and CO_2 laser, respectively. According to results of the pre-experiment and the simulate calculation, the applied filler wires are Tehan-4043 aluminum alloy with diameters of 1.0 mm and 1.2 mm. The chemical compositions of the substrate material and the filler wire are listed in Table 1 and the experiment setup for the T-joint welding is described in Figure 1. The Nd:YAG laser beam formed an angle of β (45°) with the skin and θ (25°) for the CO_2 laser, filler wire were held at the angle of 11° to the stringer at the side of Nd:YAG but perpendicular to the stringer at the CO_2 side. The symbols h and d represent the position of laser focused on the stringer and the distance between two laser beams, respectively. Before welding, plate surface was cleaned by abrasive paper and then washed by a sodium hydroxide solution followed by nitric acid to remove and minimize the oxide film.

Macrographs and microstructure observation were performed using optical micrographs. Micro-Vickers hardness was tested on the cross-section of the welded T-joints using a load of 300 g for 15 s. The T-joint tensile tests were carried out on Zwick Z020 E-stretching machine at a strain rate of 0.5 mm/min by a home-made device for clamping specimens. According to the routine operating general recognized in aeronautic industry, the specimen geometry for T-joint tensile test and the schematic description of the self-made clamping device were shown in Figures 2 and 3, respectively.

3. Experimental Results and Discussions

3.1. Appearance of the Weld. In our pre-experiments, deep penetration cannot be produced by 3 kW Nd:YAG due to the low power density. However, by preheating of tested plate, the weld depth can be increased significantly. For example, the sample preheating at 300°C showed an depth of the weld bead twice as deep as the sample without preheating, 1.00 mm versus 0.53 mm at the same welding condition (laser power = 2.8 Kw, welding speed = 1 m/min). Taking this fact into account, the Nd:YAG laser beam was placed behind CO_2 laser beam to facilitate preheating and its output was kept at 2.8 kW. The feed rate of the filler wire and the BOF were maintained at 1.4 m/min and 0.5 mm because of its minimal affection. To simplify the discussion, the wire feeding speed at the side of CO_2 laser was also kept at a constant value of 4.2 m/min.

Table 2: Influence of the distance between two laser beams on welding process (welding parameters: P_{CO_2} = 7.8 KW, υ = 4 m/min).

The distance between two laser beams	Welding process
0~1.0 mm	Unstable
1.0~1.5 mm	Stable
1.5~3.0 mm	Unstable

It is well know that the distance between two laser beams plays an important role on the welding result. Therefore, different distances have been tested from 0 to 3 mm in order to investigate the effect of this parameter on the stability of the welding. As Table 2 shows, when the distance between two laser beams is relatively small (0~1.0 mm), the absorption of Nd:YAG laser power increased and the welding seam got deeper and wider. However, smaller distance caused higher instability of welding process; this problem existed due to less preheating of the plate at the position of Nd:YAG laser focus and therefore incomplete melting of filler wire, which then resulted in blocking of wire feed and breaking off the welding process. If the distance is too big (1.5~3.0 mm), the plate also could not be preheated enough to acquire deep penetration. The distance between two laser beams which ranged from 1.0 to 1.5 mm was suitable to get stable welding processing and proper weld formation. Based on that, in the following experiment the distance between two laser beams was set as 1.5 mm.

T-joints were successfully welded with welding speed of 2 to 6 m/min and the CO_2 laser power of 7.8 kW. The typical macrographs of weld cross-sections were shown in Figure 4. It can be seen that weld seam at the side of CO_2 laser (left side in each photo) was wider than that of Nd:YAG because of the relatively higher energy input of CO_2 laser. Meanwhile, with the increased welding speed, the welding seam changed from full, wide penetration to partial, small penetration. The undercut is seen in Figures 4(a) and 4(d), but the reason is different. In the lower welding speed, the undercut is formed because of the evaporation of melted metal. While welding in the higher speed, undercut also formed for the fast cooling speed and inadequate filler wire. According to the pre-experiment, porosity is not the main problem in the whole welding processing. In general, the porosity is reduced with the increasing welding speed, because the flow of the melted metal improved and the gas can escape more easily. However, when the welding speed is too high, gas can not escape from the pool in the limited time and the amount of porosity increased. Weld beam with full penetration is useful

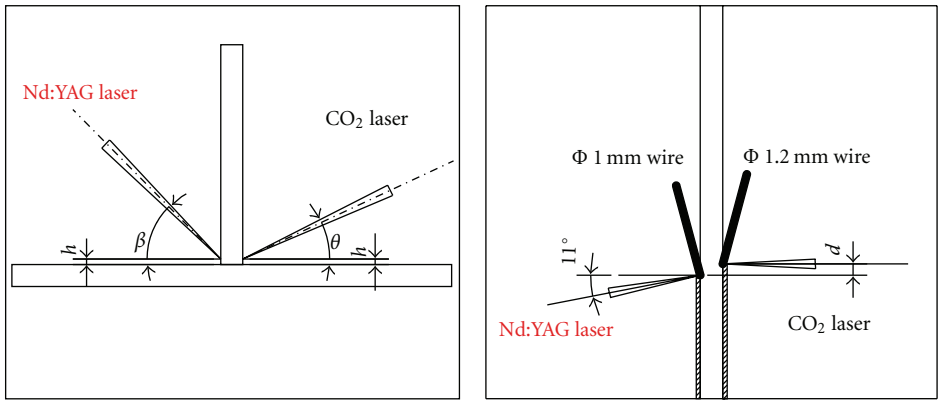

Figure 1: Schematic diagram of the experiment set-up used for the T-joint experiment.

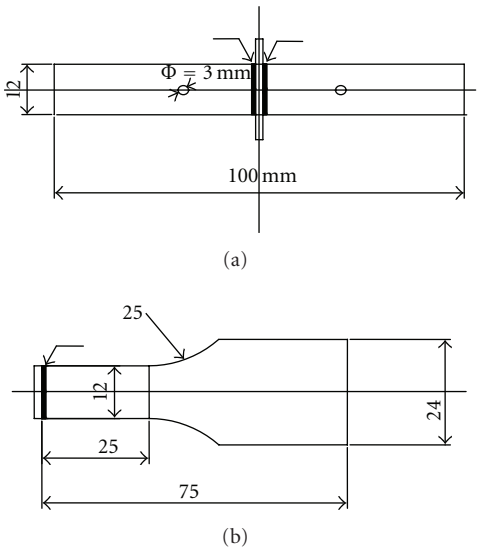

Figure 2: Specimen geometry for T-pull test.

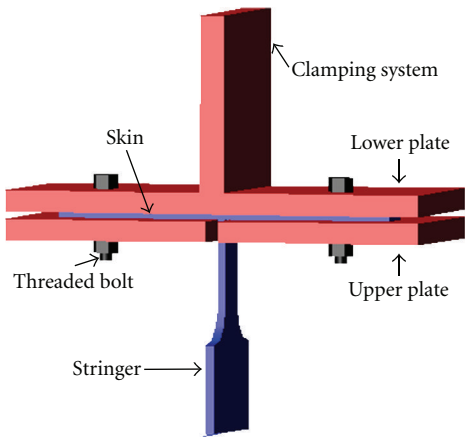

Figure 3: Self-made lamping system adopted to perform T-pull test.

to reduce the porosity. Welding speed range of 3 m/min to 4 m/min was suitable to form a sound weld seam.

The weld cross sections at different CO_2 laser power at the same welding speed of 4 m/min are shown in Figure 5. It can be found that with the increased laser power, the weld seam at CO_2 laser side became larger, but little change at the side of Nd:YAG laser was observed. When the CO_2 laser power is relatively low, the weld seam at both sides was similar, but incomplete penetration was formed as shown in Figures 5(a) and 5(b) with the red arrow pointed out. The unpenetrated fusion hindered the escape of gas with a result of higher porosity. With the increase of laser power, weld seam area at CO_2 laser side became much larger than Nd:YAG. When the laser power increased to 8.0 kW, undercut took place at CO_2 laser side, as show in Figure 5(e). As shown in Figures 5(c) and 5(d), with the laser power of 7.5 kW and 7.8 kW, sound weld seams without macrodefects were formed.

When laser spot focuses on joint of the stringer and the skin (BOF = 0 mm), any tiny change may cause large fluctuation of the weld pool, which will lead to an unstable welding process. However, the offset of laser beam toward the stringer can stabilize the welding process. Table 3 presented the widths of upper and inner fillet weld leg fabricated using BOF of 0, 0.5, and 1.0 mm at the CO_2 laser side, respectively. It can be seen that the widths of upper and inner weld leg were not symmetry and the ratio of upper and inner weld leg width was 1.35 when the BOF was 1.0 mm. Besides, there was undercut in the stringer (see in Figure 5(e)). When BOF was 0.5 mm, upper and inner weld legs of weld beam were symmetrical without any obvious defect.

3.2. Microstructures. The optical micrograph, as shown in Figure 6(a), reveals the whole view of the T-joint. While high-magnification images of spot A, B, C, and D in Figure 6(a) were shown as Figures 6(b), 6(c), 6(d), and 6(e), respectively. At the center of welding seams, very fine cellular-dendrite structures are found. The grain size at the side of Nd:YAG welding seam is a little smaller than that at CO_2

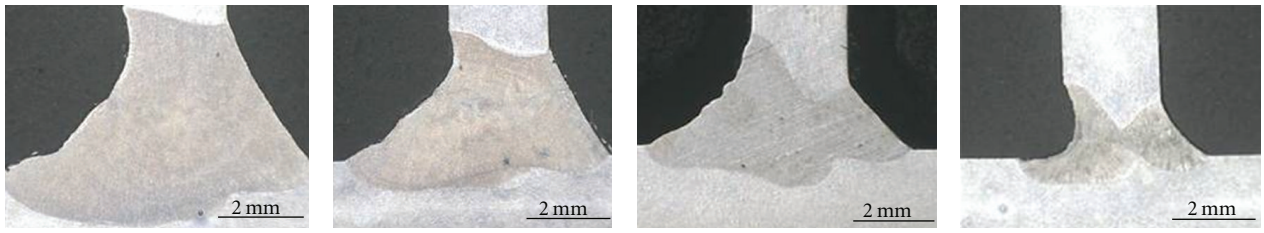

Figure 4: Macrographs of the weld seams obtained at different welding speed (fixed welding parameter: P_{CO_2} = 7.8 kW). (a) 2 m/min, (b) 3 m/min (c) 4 m/min, (d) and 6 m/min.

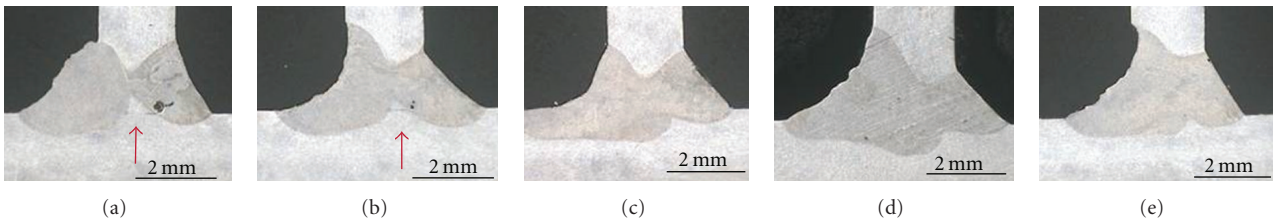

Figure 5: Macrographs of the weld seams obtained using different laser power of CO_2 laser (fixed welding parameter: υ = 4 m/min). (a) 6.8 KW, (b) 7.2 KW, (c) 7.5 KW, (d) 7.8 KW, and (e) 8.0 KW.

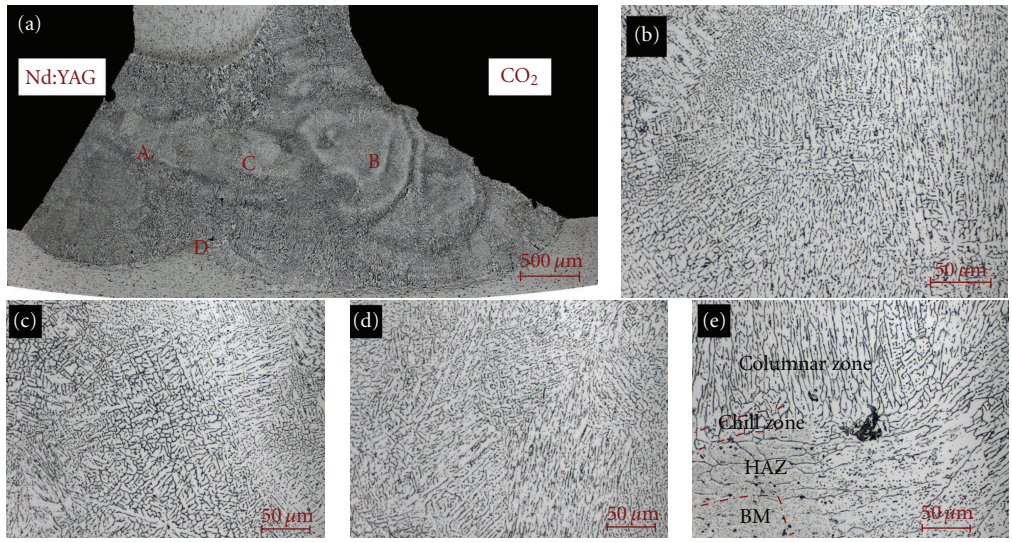

Figure 6: OM micrographs of T-joint (welding parameter: P_{CO_2} = 7.8 KW, υ = 4 m/min). (a) Macrographs of the weld seam; (b) high magnification of spot A; (c) high magnification of spot B, (d) high magnification of spot C, and (e) High magnification of spot D.

Table 3: Influence of BOF on the width of upper/down fillet weld leg and welding process (welding parameters: P_{CO_2} = 7.8 KW, υ = 4 m/min).

BOF (mm)	Upper fillet weld leg width (mm)	Down fillet weld leg width (mm)	Ration of upper/down weld leg width	Welding process
0	1.55	2.29	0.67	Unstable
0.5	2.28	2.25	1.01	Stable
1.0	2.03	1.50	1.35	Stable

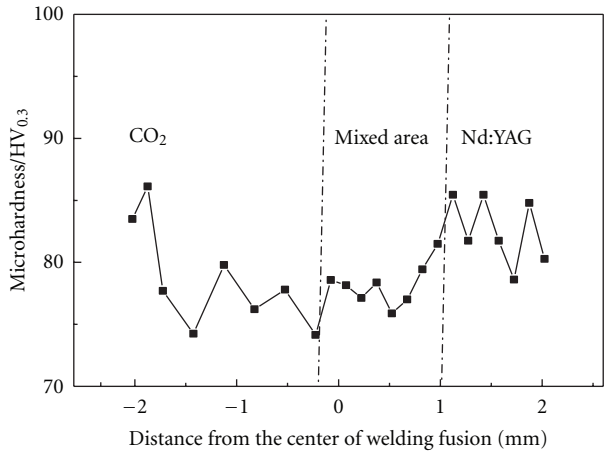

Figure 7: Microhardness of the welding seam (welding parameter: $P_{CO_2} = 7.8$ KW, $\upsilon = 4$ m/min).

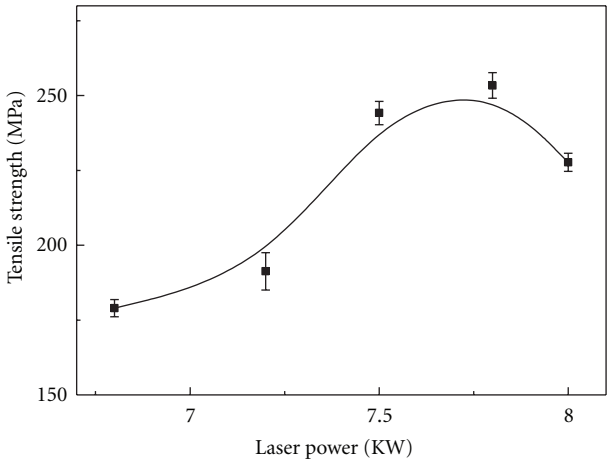

Figure 8: Relationship between tensile strength and laser power at the welding speed of 4 m/min.

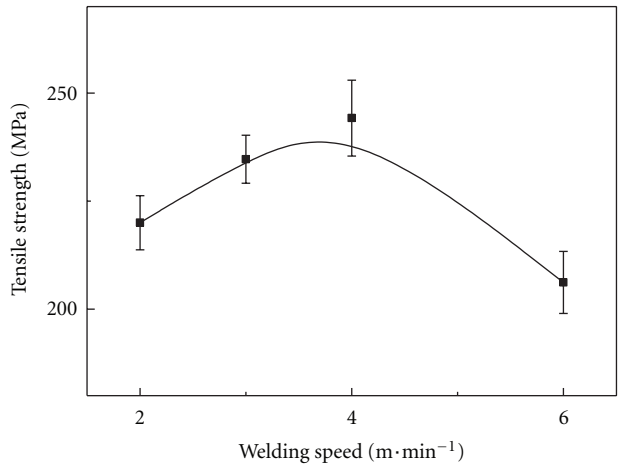

Figure 9: Relationship between tensile strength and welding speed at the laser power of 7.8 kW.

laser side due to less laser energy input. The root area of the mixed welding seam as shown in Figure 6(e) contains several distinct microstructure zones from the fusion zone to the base material. They are (1) columnar zone, parallel dendrites preferentially grew along the heat flow direction; (2) chill zone, small equiaxed grain formed; (3) heat affected zone (HAZ), the grain grow coarse to the equiaxed grain; (4) base material region (BM). The detail is drawn by the dotted line.

Varieties of microstructures were due to the different cooling rate and heat transfer direction. The morphology of the solidification structures developed in the fusion zone was controlled by the parameter G/R (G is the thermal gradient in the liquid and R is the solidification growth ratio) and the undercooling level. At the center of fusion zone, G/R reached a minimum value. While close to the fusion line, it gained its maximum in the columnar zone, with the microstructure changed from the cellular-dendrite at the center of fusion zone to parallel dendrites. Near the fusion line, the melted metal has high undercooling level, forming fine equiaxed grain (show in Chill zone). The grain in the HAZ have been affected by the thermal circle and grown coarse.

3.3. Microhardness. Figure 7 shows the microhardness profile across the weld bead of the T-joint with the CO_2 laser power of 7.5 kW. At the side of Nd: YAG fusion zone, hardness is slight higher than other area, because of low heat input resulting in smaller grain size. At the side of the CO_2 fusion zone, the micro-hardness is the lowest, for heat input is higher and the grain grows coarse. However, near the surface of the weld bead at the side of CO_2 laser, the micro-hardness increased sharply because of the fast cooling speed and small grain obtained. In the mixed area, the value of micro-hardness is between those of Nd: YAG laser and CO_2 laser. The result of micro-hardness coincides well with the grain size as Section 3.2 described.

3.4. Tensile Strength. Figures 8 and 9 show the tensile strength plot against laser power and welding speed, respectively. When the laser power was relatively low, the T-joint exhibited lower tensile strength because of nonfusion. The peak tensile strength located at about 7.5 kW to 7.8 kW, which corresponded to the complete penetration without any obvious defect. If the laser power is kept increased, the tensile strength decreased because of the grown grain size and undercut. The plot of tensile strength against welding speed is similar to Figure 8 for the same reason as discussed above. With the welding speed increased, tensile strength got maximum value at 4 m/min and then decreased, and the peak tensile strength was 254 MPa with the fracture at the heat affected zone (HAZ) on the stringer side.

4. Conclusions

(1) The parameters such as distance between two laser beams (d), welding speed (υ), laser power (P), and the laser beam offset toward the stringer (BOF) was systematically investigated. The results showed that

these parameters have great effect on the stability and macrostructure of the welding.

(2) The undercut would be occurred under relatively high and low welding speed as well as higher laser power. Complete penetration is helpful to reduce the porosity.

(3) With the optimized parameters (d = 1.0~1.5 mm, v = 3~4 m/min, P_{CO_2} = 7.5 ~ 7.8 kW, BOF = 0.5), T-joint with good weld appearance, no obvious porosity, and undercut was observed.

(4) Micrograph observation showed the joint had different distinct zone with different microstructure from the center of fusion zone to the BM. At the center of fusion zone, cellular dendrites are present. While close to the fusion line, microstructure changes to parallel dendrites for preferentially elongating along the heat flow direction. In chill zone, fine equiaxed grain formed due to high undercooling level. In the HAZ, grain grew coarse for the thermal circle.

(5) Micro-hardness at the Nd:YAG zone is higher than other area due to smaller grain size. The tensile strength was about 254 MPa with the fracture at the heat affected zone (HAZ) on the stringer side.

References

[1] M. Zain-ul-abdein, D. Nélias, J. F. Jullien, and D. Deloison, "Experimental investigation and finite element simulation of laser beam welding induced residual stresses and distortions in thin sheets of AA 6056-T4," *Materials Science and Engineering A*, vol. 527, no. 12, pp. 3025–3039, 2010.

[2] C. Williams, "CO_2 laser processing—an overview," *Aircraft Engineering and Aerospace Technology*, vol. 69, no. 1, pp. 43–52, 1997.

[3] X. Cao, W. Wallace, C. Poon, and J. P. Immarigeon, "Research and progress in laser welding of wrought aluminum alloys. I. Laser welding processes," *Materials and Manufacturing Processes*, vol. 18, no. 1, pp. 1–22, 2003.

[4] E. Schubert, M. Klassen, I. Zerner, C. Walz, and G. Sepold, "Light-weight structures produced by laser beam joining for future applications in automobile and aerospace industry," *Journal of Materials Processing Technology*, vol. 115, no. 1, pp. 2–8, 2001.

[5] M. Zain-ul-Abdein, D. Nelias, J. F. Jullien, and D. Deloison, "Prediction of laser beam welding-induced distortions and residual stresses by numerical simulation for aeronautic application," *Journal of Materials Processing Technology*, vol. 209, no. 6, pp. 2907–2917, 2009.

[6] S. Daneshpour, M. Koçak, F. S. Bayraktar, and S. Riekehr, "Damage tolerance analyses of laser welded "skin-clip" joints for aerospace applications," *Welding in the World*, vol. 53, no. 3-4, pp. R90–R98, 2009.

[7] F. S. Bayraktar, P. Staron, M. Koçak, and A. Schreyer, "Analysis of residual stress in laser welded aerospace aluminium T-joints by neutron diffraction and finite element modelling," *Materials Science Forum*, vol. 571-572, pp. 355–360, 2008.

[8] E. M. Van der Aa, *Local cooling during welding: prediction and control of residual stresses and buckling distortion*, Ph.D. thesis, Delft University of Technology, Delft, The Netherlands, 2006.

[9] K. Masubuchi, *Analysis of Welded Structures*, Pergamon Press, New York, NY, USA, 1980.

[10] M. V. Deo and P. Michaleris, "Mitigation of welding induced buckling distortion using transient thermal tensioning," *Science and Technology of Welding and Joining*, vol. 8, no. 1, pp. 49–54, 2003.

[11] W. Machold, W. Staron, P. Bayraktar, F. Riekehr, S. Kocak, and M. Schreyer, "Influence of the welding sequence on residual stresses in laser welded t-joints of an airframe aluminum alloy," *Stress Evaluation in Materials using Neutrons and Synchrotron Radiation*, vol. 571-72, pp. 375–380, 2008.

[12] T. Schenk, M. Doig, G. Esser, and I. M. Richardson, "Influence of clamping support distance on distortion of welded T joints," *Science and Technology of Welding and Joining*, vol. 15, no. 7, pp. 575–582, 2010.